Functions of maize genes encoding pyruvate phosphate dikinase in developing endosperm

Ryan R. Lappe[a], John W. Baier[b], Susan K. Boehlein[b], Ryan Huffman[c], Qiaohui Lin[a], Fabrice Wattebled[d], A. Mark Settles[b], L. Curtis Hannah[b], Ljudmilla Borisjuk[e], Hardy Rolletschek[e], Jon D. Stewart[f], M. Paul Scott[c,g], Tracie A. Hennen-Bierwagen[a], and Alan M. Myers[a,1]

[a]Roy J. Carver Department of Biochemistry, Biophysics, and Molecular Biology, Iowa State University, Ames, IA 50011; [b]Horticultural Sciences Department, University of Florida, Gainesville, FL 32611; [c]Department of Agronomy, Iowa State University, Ames, IA 50011; [d]Univérsité de Lille, CNRS, UMR 8576, Unité de Glycobiologie Structurale et Fonctionnelle, F 59000 Lille, France; [e]Department of Molecular Genetics, Leibniz Institute of Plant Genetics and Crop Plant Research, D-06466 Gaterslaben, Germany; [f]Department of Chemistry, University of Florida, Gainesville, FL 32611; and [g]Corn Insects and Crop Genetics Unit, US Department of Agriculture-Agricultural Research Service, Ames, IA 50011

Edited by Brian A. Larkins, University of Nebraska, Lincoln, NE, and approved November 27, 2017 (received for review September 7, 2017)

Maize *opaque2* (*o2*) mutations are beneficial for endosperm nutritional quality but cause negative pleiotropic effects for reasons that are not fully understood. Direct targets of the bZIP transcriptional regulator encoded by *o2* include *pdk1* and *pdk2* that specify pyruvate phosphate dikinase (PPDK). This enzyme reversibly converts AMP, pyrophosphate, and phosphoenolpyruvate to ATP, orthophosphate, and pyruvate and provides diverse functions in plants. This study addressed PPDK function in maize starchy endosperm where it is highly abundant during grain fill. *pdk1* and *pdk2* were inactivated individually by transposon insertions, and both genes were simultaneously targeted by endosperm-specific RNAi. *pdk2* accounts for the large majority of endosperm PPDK, whereas *pdk1* specifies the abundant mesophyll form. The *pdk1*- mutation is seedling-lethal, indicating that C4 photosynthesis is essential in maize. RNAi expression in transgenic endosperm eliminated detectable PPDK protein and enzyme activity. Transgenic kernels weighed the same on average as nontransgenic siblings, with normal endosperm starch and total N contents, indicating that PPDK is not required for net storage compound synthesis. An opaque phenotype resulted from complete PPDK knockout, including loss of vitreous endosperm character similar to the phenotype conditioned by *o2*-. Concentrations of multiple glycolytic intermediates were elevated in transgenic endosperm, energy charge was altered, and starch granules were more numerous but smaller on average than normal. The data indicate that PPDK modulates endosperm metabolism, potentially through reversible adjustments to energy charge, and reveal that *o2*- mutations can affect the opaque phenotype through regulation of PPDK in addition to their previously demonstrated effects on storage protein gene expression.

maize | endosperm | metabolism | opaque | PPDK

Maize *opaque2* (*o2*) mutations condition desirable changes in grain amino acid balance, yet also cause floury, opaque grain quality rather than agronomically optimal vitreous character. *o2* encodes a bZIP transcription factor that directly regulates multiple targets in endosperm including α-, β-, and γ-zein proteins, the starch synthase SSIIIa, and pyruvate phosphate dikinase (PPDK) (EC 2.7.9.1) (1, 2). PPDK and SSIIIa may cooperate in some functions because they associate in multisubunit complexes in developing endosperm (3). Determining the functions of each target is necessary to understand fully how *o2*- affects grain quality and in turn how to best achieve nutritional quality traits. The effects of zein deficiencies and SSIIIa mutations have been characterized (4–6), but maize endosperm PPDK function has not been described.

PPDK reversibly interconverts pyruvate, ATP, and orthophosphate with phosphoenolpyruvate (PEP), AMP, and pyrophosphate (PPi) (7–9) and provides diverse functions in various plant tissues. CO_2 fixation via the C4 pathway utilizes PPDK in mesophyll chloroplasts to regenerate the initial carboxylate group acceptor PEP (10–12). PPDK also functions in senescing leaves, converting pyruvate from amino acid breakdown to PEP in a pathway yielding glutamine for amino group transport (13). This involves cytosolic PPDK, rather than the plastidial form involved in C4 metabolism. Cytosolic PPDK also functions in gluconeogenesis during *Arabidopsis* seed germination, using pyruvate from amino acid catabolism (14). Another function is to provide PEP to the shikimate pathway in cells surrounding the vasculature, using pyruvate from decarboxylation of organic acids in the transpiration stream (15).

In the preceding instances, PPDK acts in the gluconeogenic direction, converting pyruvate to PEP and consuming ATP. PPDK can also act glycolytically, for example, in microorganisms in anoxic or hypoxic environments, and sometimes replaces pyruvate kinase in glycolysis (16). This reaction yields 2 mol ATP per mol PEP when adenine nucleotide equilibration by adenylate kinase is considered, rather than 1 mol ATP in canonical glycolysis, and this can be advantageous in oxygen-limiting conditions (16, 17). Potential glycolytic function of PPDK in plants is suggested by its markedly increased expression in rice coleoptiles or seedlings subjected to anoxia (18, 19). Maize endosperm is another oxygen-limited tissue with high PPDK levels (20–22), coincident with biomass accumulation and associated ATP demand. Direct evidence of PPDK

Significance

Mutations affecting the transcription factor encoded by the gene *o2* are important in maize agriculture because they result in improved grain nutritional quality. The mutations also cause detrimental effects by reducing kernel hardness and diminishing agronomic quality and food applications. The undesirable characteristics are not fully understood because the *o2* product regulates multiple targets that could contribute to the phenotype. This study investigated one target that had not been previously mutated, pyruvate phosphate dikinase (PPDK), and showed that PPDK deficiency in isolation causes the negative phenotype associated with reduced kernel hardness. Thus, maize improvement may be better accomplished by targeting individual metabolic pathways determining protein and amino acid balance rather than pleiotropic regulators such as the *o2* transcription factor.

Author contributions: R.R.L., S.K.B., A.M.S., L.C.H., J.D.S., M.P.S., T.A.H.-B., and A.M.M. designed research; R.R.L., J.W.B., S.K.B., R.H., Q.L., F.W., L.B., H.R., J.D.S., T.A.H.-B., and A.M.M. performed research; R.R.L., Q.L., and L.B. contributed new reagents/analytic tools; R.R.L., J.W.B., S.K.B., F.W., A.M.S., L.B., H.R., J.D.S., M.P.S., T.A.H.-B., and A.M.M. analyzed data; and R.R.L., T.A.H.-B., and A.M.M. wrote the paper.

The authors declare no conflict of interest.

This article is a PNAS Direct Submission.

[1]To whom correspondence should be addressed. Email: ammyers@iastate.edu.

This article contains supporting information online at www.pnas.org/lookup/suppl/doi:10.1073/pnas.1715668115/-/DCSupplemental.

www.pnas.org/cgi/doi/10.1073/pnas.1715668115

function in plant glycolysis is lacking, however, and any role in low-oxygen conditions remains to be determined. Other hypotheses for endosperm PPDK function include (*i*) gluconeogenesis, providing hexose for starch biosynthesis; (*ii*) provision of pyruvate for lipid synthesis; and (*iii*) control of metabolic fluxes through its contribution to PPi homoeostasis (3, 19, 21, 23, 24). The latter hypothesis considers that PPi is a product of both PPDK's gluconeogenic activity and ADP glucose pyrophosphorylase that routes glucose-phosphate into starch metabolism.

Mutation of one of the two rice PPDK genes conditioned opaque endosperm (24). Thus, *o2*- could conceivably cause opaque endosperm entirely through PPDK, independent of its effects on zein expression and starch biosynthesis. Net biomass incorporation was only slightly reduced in rice PPDK single mutants, showing that ATP produced by PPDK is not a major contributor to overall anabolic metabolism. Further analysis is needed, however, because the second rice PPDK gene remained active, endosperm PPDK expression varies between maize and rice, and the metabolic basis of the change from vitreous to floury tissue character remains unknown. The current study transgenically eliminated PPDK from maize endosperm and classically inactivated each of the two maize PPDK genes. Endosperm PPDK knockout caused mutation from vitreous to opaque kernel character, and metabolite analyses indicated that PPDK affects glycolysis and the energy charge, i.e., the ratio of ATP to ADP + AMP. The results emphasize the pleiotropic nature of *o2*- effects on grain quality, including storage protein accumulation, starch biosynthesis, and metabolic regulation mediated by PPDK.

Results

Insertional Mutagenesis of *pdk1* and *pdk2*. The maize genome contains two loci encoding PPDK, designated here *pdk1* (gene model GRMZM2G306345) and *pdk2* (gene model GRMZM2G097457). The *pdk1* locus utilizes alternative start sites, with one mRNA encoding a predicted plastid transit peptide and the other lacking codons for any obvious targeting signal (25). *pdk2* encodes a predicted cytosolic protein that is 94% identical to the cytosolic *pdk1* product. Transposon insertion alleles of *pdk1* and *pdk2* were isolated. *pdk1-MuEx10* contains a *Mutator* (*Mu*) element in exon 10, and *pdk2-DsEx4* is caused by a *Dissociation* element (*Ds*) in exon 4 (Fig. 1*A*). Each mutation was maintained in heterozygotes through at least five backcrosses to standard inbred W64A for *pdk1-MuEx10* or W22D (26) for *pdk2-DsEx4*. Crosses between heterozygotes generated homozygous mutant and nonmutant sibling kernels on the same ear, genotyped by PCR (*SI Appendix*, Fig. S1*A*). Visual kernel phenotypes were not observed, nor did kernel weight differ between mutant and wild-type seeds on the same ear (*SI Appendix*, Table S1). This is in contrast to rice, where a single mutant lacking function of the *pdk1* homolog caused an opaque phenotype (24). Single-kernel near infrared reflectance (NIR) spectra predicted starch, protein, and oil content, as well as density, in the segregating

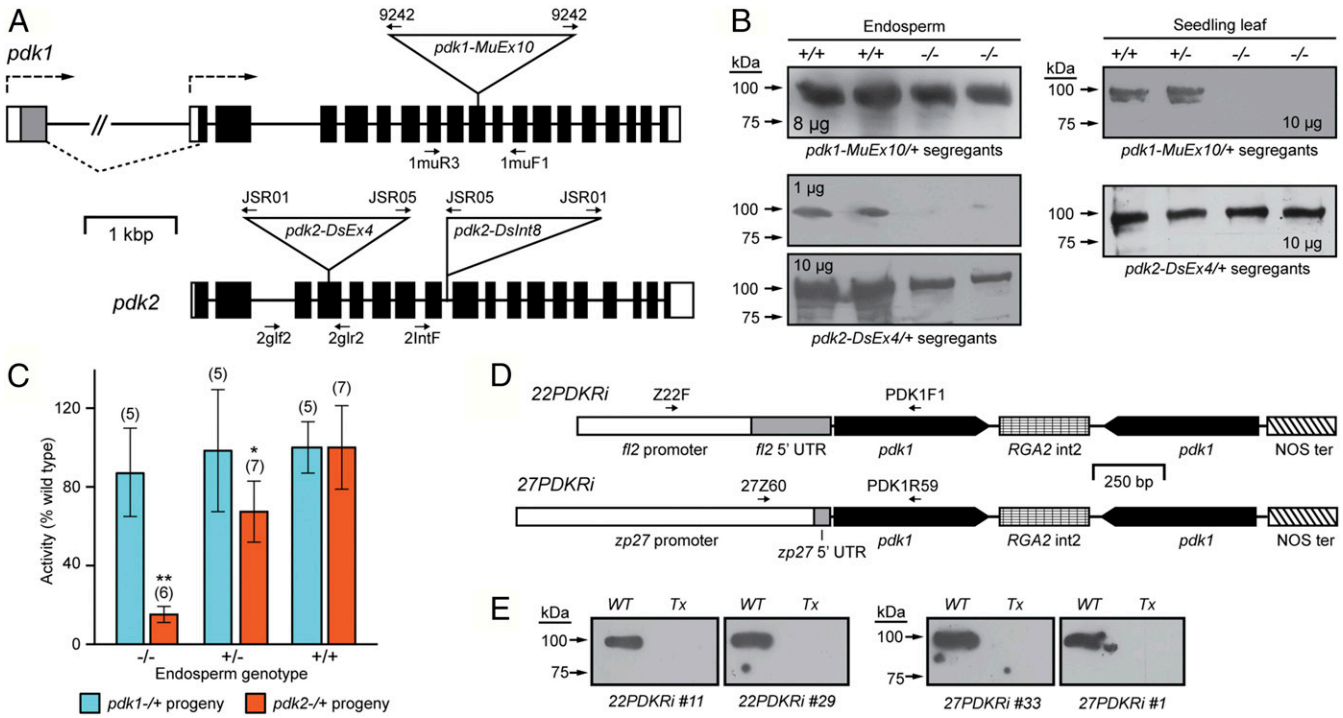

Fig. 1. Alleles, transgenes, and effects on PPDK expression. (*A*) Gene maps. White boxes represent untranslated regions, gray and black boxes represent coding regions, and solid lines represent introns. The figure is to scale except for *pdk1* intron 1 and the *Mu* or *Ds* insertions. Dashed arrows indicate two transcription start sites in *pdk1*, the gray box represents the transit peptide-encoding sequence, and dashed lines show splice junctions of the *pdk1* mRNA that contains the transit peptide codons. Solid arrows indicate PCR primers. (*B*) PPDK immunoblots of insertion mutants. The indicated amount of soluble extract was fractionated by SDS/PAGE and probed with anti-PPDK. Endosperm extracts were from sibling progeny kernels of crosses between heterozygotes harvested 20 DAP and genotyped from corresponding embryo DNA. Seedling leaf extracts were from progeny plants of crosses between heterozygotes genotyped from leaf DNA. (*C*) PPDK enzyme activity in endosperm extracts of insertion mutants. Endosperms were obtained as in *B*. Numbers in parentheses indicate biological replicates. Error bars show SD. Single asterisk indicates significant difference from wild type ($P = 0.007$). Double asterisk indicates significant difference from heterozygote ($P < 10^{-5}$). (*D*) Transgene structure. "*pdk1*" indicates nucleotides 114–659 of the *pdk1* cDNA (GenBank accession J03901). "RGA2 int2" indicates the second intron of the wheat *RGA2* gene. "NOS ter" is the transcriptional terminator of the nopaline synthase gene from the *Agrobacterium tumefaciens* Ti plasmid. *fl2* and *zp27* sequences are described in *SI Appendix, SI Materials and Methods*. (*E*) PPDK immunoblots of transgenic endosperm. Hemizygotes were crossed to a standard inbred, and progeny kernels were classified by PCR as containing (*Tx*) or lacking (*WT*) the indicated transgene. Immunoblot analysis was as in *A*, with 5-µg protein loaded.

populations (27, 28). No consistent differences between wild-type and mutant siblings were observed regarding composition, although NIR spectra differences correlated with elevated density in *pdk2-DsEx4* homozygous kernels (*SI Appendix*, Table S1).

Single-mutant plants were also examined for phenotypic effects. Homozygous *pdk1-MuEx10* plants germinated normally (*SI Appendix*, Fig. S2*A*), but seedlings invariably died at the three-leaf stage (*SI Appendix*, Fig. S3). Necrosis was first evident in leaf tips, coincident with cells in normal plants that initially acquire C4 metabolism (29). This confirms that *pdk1-MuEx10* is a loss-of-function allele and indicates that C4 metabolism is essential for maize viability. Homozygous *pdk2-DsEx4* plants germinated normally (*SI Appendix*, Fig. S2*B*), were viable, and displayed no obvious growth or morphological phenotype.

PPDK protein levels in wild-type and mutant sibling endosperms were measured by immunoblot. Homozygous *pdk2-DsEx4* mutants exhibited strongly reduced PPDK signal, although residual protein was detected when gel lanes were overloaded with a 10-fold increase of total extract (Fig. 1*B*). This major effect on PPDK level confirms that *pdk2-DsEx4* is a loss-of-function allele. The result further indicates that *pdk1* conditions a minor portion of the endosperm enzyme, consistent with proteomic data showing PPDK1 to be 5% of the total (22) and enzyme activity data that follows. Loss of *pdk1* function had no obvious effect on endosperm PPDK level, consistent with each form's abundance indicated from proteomic analysis. Transcriptomic data show *pdk2* transcripts are approximately three- to seven-fold more abundant in endosperm than *pdk1* transcripts during the grain-filling stage of 12–30 days after pollination (DAP) (30, 31), so for these genes there is a general correlation between steady-state mRNA level and protein concentration.

Leaf PPDK levels were measured similarly. *pdk1-MuEx10* conditioned an apparently complete loss of PPDK immunoblot signal in seedling leaf, whereas *pdk2-DsEx4* had no detectable effect (Fig. 1*B*). This is consistent with proteomic observation of PPDK1 at a high level in mesophyll and of PPDK2 in much lower abundance exclusively in bundle sheath cells (32).

Endosperm PPDK activity was also measured. In agreement with immunoblot data, homozygous *pdk2-DsEx4* conditioned ~85% reduction compared with wild-type siblings, whereas *pdk1-MuEx10* had no detectable effect (Fig. 1*C*). Enzyme activity is proportional to gene dosage as shown by 33% reduction in heterozygous *pdk2-DsEx4*/+ endosperm compared with +/+. This confirms that *pdk2* is the major contributor to total endosperm PPDK function. Remnant activity in *pdk2-DsEx4* homozygotes confirms that *pdk1* contributes a minor fraction of the total.

RNAi-Mediated Inhibition of Endosperm PPDK Expression. Tissue-specific RNAi was used to target both *pdk1* and *pdk2* for inactivation with a single transgene while circumventing seedling lethality caused by *pdk1* mutation in vegetative tissue. Endosperm-specific promoters from the gene *zp27* encoding the 27-kDa γ-zein (33), or *Fl2* encoding a highly expressed 22-kDa α-zein (34), directed expression of a 546-bp segment of the *pdk1* cDNA-coding region duplicated in inverted orientation (Fig. 1*D*) (*SI Appendix*, Fig. S4). The expressed sequence contains 323 bp that are 95% identical in the *pdk1* and *pdk2* cDNAs (*SI Appendix*, Fig. S5), so the transgenes target both loci. Significantly similar sequence does not appear elsewhere in the maize inbred B73 genome. Both promoters are active apparently exclusively in endosperm starting early during grain fill and maintain function throughout development (30, 33, 35). Three lines with independent integrations of transgene *27PDKRi*, containing the *zp27* promoter, and two lines with independent integrations of *22PDKRi*, containing the *Fl2* promoter, were backcrossed into W64A or B73 inbred backgrounds. PCR genotyping (*SI Appendix*, Fig. S1*B*) revealed near-Mendelian ratios of progeny lacking or containing each transgene, demonstrating a single genomic locus for each insertion. Transgene-containing plants germinated and developed apparently normally in field conditions as far as visual characterization can determine. Germination frequency was assayed directly, with no differences detected between transgenic kernels and wild-type siblings (*SI Appendix*, Fig. S2*C*). Plant viability and apparently normal growth rates indicated that transgene expression is limited to endosperm.

Immunoblot analysis evaluated the effects of each transgene on endosperm PPDK level. Hemizygotes were crossed to wild type to generate segregating populations of transgenic and normal sibling kernels on the same ear. PPDK was readily detectable in normal segregants but was not observed in transgenic siblings bearing any of four independent transgenes (Fig. 1*E*). PPDK enzyme activity in transgenic endosperm extracts from all five lines was undetectable above background (*SI Appendix*, Table S2). Thus, *27PDKRi* and *22PDKRi* cause endosperm PPDK reduction to below detectable levels and so are considered to cause complete or near-complete knockout of the enzyme in that tissue.

Kernel Phenotypes Mediated by PPDK Deficiency. Hemizygous plants in the B73 or W64A background were crossed to the reciprocal standard to generate <B73/W64A> F_1 ears with kernels segregating for presence or absence of the transgene. Progeny kernels were analyzed visually for opaque appearance by NIR spectroscopy to predict density and composition and by PCR genotyping. Strong correlation was observed between the transgene, opaque appearance, and reduced predicted kernel density (Fig. 2 *A* and *B*) (*SI Appendix*, Table S3). Exceptions likely were from incomplete penetrance or incorrect scoring for phenotype or genotype, as shown by χ^2 tests (*SI Appendix*, Table S4). Essentially the same phenotypes were observed in inbred genetic backgrounds as well as the hybrid, over successive field seasons, and were conditioned by five independent transgene events (*SI Appendix*, Fig. S6 and Table S3). The transgenes caused essentially complete loss of vitreousness in the <B73/W64A> F_1 or B73 inbred background, whereas in the W64A background the vitreous region was reduced compared with normal, rather than eliminated (Fig. 2*A*) (*SI Appendix*, Fig. S6).

Distinctions in packing of storage compounds were also detected by magnetic resonance imaging (MRI) that measures ^{1}H NMR signal over virtual cross-sections (Fig. 2*C*). The parameters result in attenuated signals from compounds with long relaxation times, e.g., free water and lipid, whereas components with short relaxation times, e.g., starch, proteins, bound water, or sugars, contribute to the measurement (36). Wild-type kernels exhibited areas of high NMR signal at the endosperm periphery alternating with low intensity signal in the interior, correlating with vitreous and floury tissue, respectively. In contrast, transgenic segregants exhibited essentially uniform signal intensity across the section at the level corresponding to the interior floury area of nonmutant siblings.

Protein content differences between transgenic and normal kernels were predicted from NIR spectra in 9 of 10 ears, and oil content variation in 7 ears (*SI Appendix*, Table S3). Mature kernel weight did not vary by genotype in any segregating population (*SI Appendix*, Table S3). Total endosperm nitrogen and starch were measured directly in families segregating for *27PDKRi #1*. In two ears harvested 20 DAP, and in one mature ear, no significant difference in total N content determined by elemental analysis was detected (*SI Appendix*, Table S5). Starch content was determined in single endosperms from the mature ear and one 20-DAP ear. Again, significant differences between transgenic and normal endosperms were not detected (*SI Appendix*, Table S5). The observations that total N and starch in endosperm are unchanged, yet NIR spectra predict elevated protein content in whole kernels of transgenic segregants, may indicate altered endosperm-to-embryo ratio within mature seed.

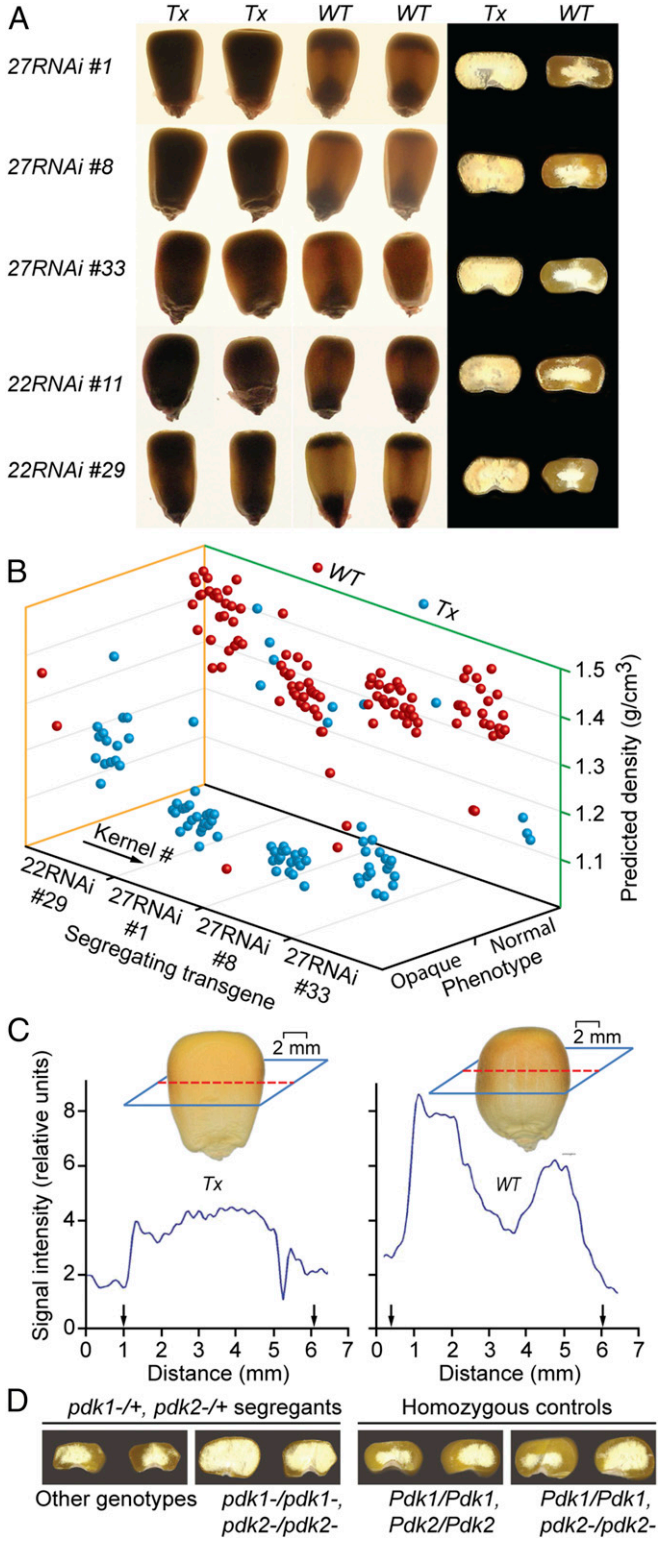

Fig. 2. Opaque phenotype conditioned by PPDK deficiency. (*A*) Visual phenotype conditioned by RNAi transgenes. Mature kernels were photographed over transmitted light, and cross-sections were imaged on a flatbed scanner. Genotypes were then determined by PCR. For each transgene, sibling kernels were from the same ear. *Tx*, transgene-containing segregants; *WT*, nontransgenic siblings. (*B*) Cosegregation of predicted density, visual phenotype, and genotype. Approximately 48 individuals from each ear, segregating for the indicated transgene, were scored visually as in *A*, analyzed by single-kernel NIR, and genotyped. Each point represents an individual kernel. (*C*) MRI determination of total spin density positioned across mature kernels. NMR signal intensity was collected in a virtual cross-section along the axis shown in the red dotted lines above each plot, in a plane that avoids the embryo. Vertical arrows indicate the position of each kernel boundary along that axis. Individuals shown are from an ear segregating for *27PDKRi #33*. (*D*) Visual phenotype conditioned by insertion mutations. Double heterozygotes (*pdk1-MuEx10*/+, *pdk2-DsEx4*/+) were crossed, and progeny kernels from the same ear were analyzed as in *A*. Nonmutant kernels and *pdk2-DsEx4* homozygous single mutants in the W22D inbred background are included as controls.

Light microscopy (LM) revealed that at maturity starch granules are packed less tightly than normal in PPDK-deficient endosperm (Fig. 3), consistent with floury texture. The granule diameter distribution at maturity was shifted toward smaller particles in transgenic kernels bearing either *27PDKRi #1* or *27PDKRi #33* compared with nontransgenic siblings (Fig. 4). The linear chain length distribution within amylopectin and the amylose content were measured in transgenic and nontransgenic kernels segregating for either *27PDKRi #1* or *27PDKRi #33*. No significant differences were detected.

No obvious differences in protein body morphology between PPDK-deficient endosperm and normal siblings were detected at the ultrastructural level (Fig. 5) (*SI Appendix*, Fig. S7). Zein content was analyzed chromatographically (*SI Appendix*, Fig. S8) and by SDS/PAGE (*SI Appendix*, Fig. S9) in lines segregating for any of three different transgenes. Included as a control was transgene *27GUS #5*, which expresses *Escherichia coli* β-glucuronidase from the *zp27* promoter. Neither total zein nor nonzein protein level was noticeably decreased between PPDK-deficient endosperm and normal siblings (*SI Appendix*, Figs. S8 and S9). One exception was noted in *27PDKRi #1* individuals where 27-kDa γ-zein was strongly reduced (*SI Appendix*, Fig. S8*E*). This was not an effect of the *zp27* promoter because neither *27PDKRi #33* nor *27PDKRi #8* nor *27GUS #5* affected that peak. The steady-state level of O2 protein detected by immunoblot was not affected by any of the transgenes (*SI Appendix*, Fig. S10), consistent with essentially normal zein protein levels.

To test the conclusion that loss of endosperm vitreousness results from PPDK deficiency, double-mutant kernels homozygous for *pdk1-MuEx10* and *pdk2-DsEx4* were generated from crosses between double-heterozygous plants. As predicted, ~1/16th of the progeny kernels exhibited strongly reduced vitreous endosperm (Fig. 2*D*), and PCR genotyping revealed these to be double mutants.

Metabolite Phenotypes Conditioned by PPDK Deficiency. Nontargeted and targeted metabolomics analyses of 20-DAP endosperm revealed changes in the levels of specific compounds in PPDK-deficient segregants relative to wild-type siblings. For nontargeted analysis, three ears were analyzed that varied by growth year, inbred background, and transgene event. For each ear, metabolites were extracted from two biological replicate pools of transgenic endosperms and two pools of nontransgenic siblings, with five individuals per pool. Metabolites in the aqueous phase of $CHCl_3$-methanol extracts were analyzed by reverse-phase liquid chromatography-electrospray ionization mass spectrometry (RPLC-MS). Integrated peak height intensity was tabulated for 700 negative ion mass features (Dataset S1) and 1,164 positive ion features (Dataset S2). Data filtering removed 25% of the negative features and 40% of the positive features before analysis (37). Principal component analysis (PCA) showed that maximum variation in global metabolite pools was between individual ears independent of kernel genotype (Fig. 6*A*). PC3 distinguished samples by genotype, indicating that PPDK loss conditioned reproducible changes in steady-state metabolite populations independently of variation between parent plants or

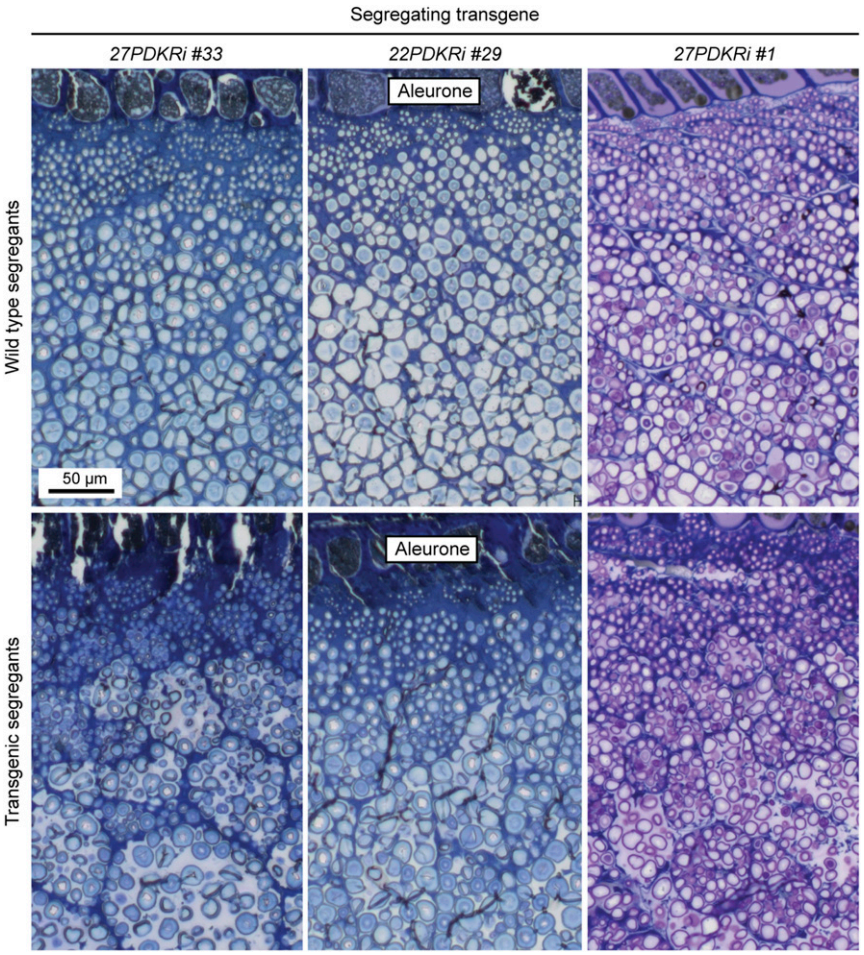

Fig. 3. LM visualization of mature endosperm. Sibling mature kernels from the same ear segregating for the indicated transgene were fixed, embedded, sectioned, stained with Toluidine blue and basic fuschsin, and visualized by light microscopy. The aleurone layer marks the exterior of the endosperm tissue. (Scale bar for all images, 50 μm.)

their environment. PCA applied to eight pools from the same field season, including two independent transgene events, found that PC2 distinguishes transgenic and nonmutant siblings, accounting for >20% of variation. Statistical analyses (*Materials and Methods*) identified specific mass features likely to vary in abundance owing to presence or absence of PPDK, some of which were identified by comparison with standards (*SI Appendix*, Table S6).

Targeted analyses quantified fold-changes in PPDK substrates and other metabolites not detected by RPLC-MS. ATP was quantified enzymatically in sibling endosperms segregating on two different ears (Fig. 6*B*). Gas chromatography-MS (GC-MS) methods were developed (*Materials and Methods*) to measure pyruvate, PEP, and PPi in total extracts (Fig. 6*C*). A targeted set of central metabolites was also analyzed by anion exchange liquid chromatography-MS (AELC-MS) (20, 38).

Steady-state concentrations of multiple glycolytic intermediates and related metabolites are elevated in the absence of PPDK (Fig. 7*A*). Glc-1-P was the most statistically significant change in the nontargeted RPLC-MS analysis, showing a 1.8-fold elevation in PPDK-deficient endosperm. Dihydroxyacetone phosphate (DHAP) exhibited a significant 5.6-fold increase. A hexose alcohol, likely sorbitol from reduction of Glc or Frc, and ribose-5-phosphate and/or ribulose-5-phosphate from Glc-1-P through the oxidative pentose phosphate pathway, were both significantly elevated in transgenic tissue. Targeted GC-MS found PEP to be significantly elevated twofold in transgenic segregants containing any of three independent transgenes (Fig. 6*C*). Pyruvate, however, was not significantly altered between transgenic and normal siblings. AELC-MS independently detected excess Glc-1-P and PEP in transgenic samples and confirmed that pyruvate levels are not significantly altered. AELC-MS revealed further that hexose-6-P and Frc-1,6-BP steady-state levels are also elevated in PPDK-deficient endosperm.

The citric acid cycle did not appear to be substantially altered by PPDK deficiency (Fig. 7*A*). RPLC-MS found citrate, succinate, fumarate, malate, and oxaloacetate all to be unaffected. The 2-oxoglutarate, however, was elevated 2.1-fold in PPDK-deficient tissue. Similar results were found independently by AELC-MS. Twelve free amino acids were identified by RPLC-MS, of which Thr, Tyr, Met, Pro, Asn, Leu, Ile, Ala, Phe, and Trp were unaffected by loss of PPDK. Gln was elevated in transgenic endosperm, consistent with increased 2-oxoglutarate, whereas Asp was reduced twofold.

Energy charge, a factor determined by the ratio of ATP to AMP and ADP, was altered in PPDK-deficient endosperm. AMP, UMP, and CMP were all significantly elevated in steady-state level in transgenic kernels (Fig. 6*B*). ADP also exhibited a large fold increase, although high variation precluded assigning statistical significance. Average ATP content was significantly reduced by 20% in transgenic endosperm ($P = 0.002$; $n = 40$) (Fig. 6*B*), consistent with AMP and ADP elevation. Finally,

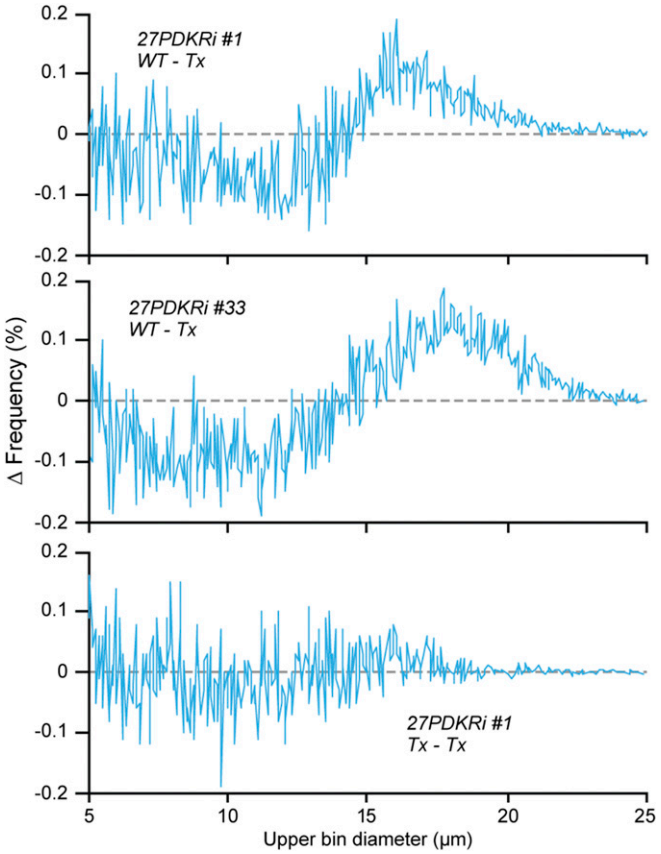

Fig. 4. Starch granule diameter differences. Granule diameters were measured by a Coulter Counter, and the abundance for each size range from 5 to 25 μm was calculated as a percentage of total. The difference in frequency for each size range was determined by subtracting the mutant value (*Tx*) from the wild-type value (*WT*). Each normal and transgenic pair were sibling endosperms from the same ear. (*Lower*) Comparison of sibling transgenic kernels from the same ear both containing *27RNAi #1* to indicate results typical for individuals of the same genotype. The pairwise comparisons shown are representative of three independent biological replicates that yielded essentially identical results.

although PPi could be detected in total extracts by both GC-MS and AELC-MS, in each instance the quantified values were too variable to assign statistical significance.

Discussion

This study demonstrates that maize endosperm PPDK is required for normal organization of storage compounds so that mature tissue achieves the hard, vitreous character necessary for optimal agronomic traits. The data imply that *o2*- mutations can affect kernel vitreousness not only through zein protein levels, but also by regulating PPDK expression (Fig. 7*B*). This provides further support for the concept that alteration of maize nutritional quality by manipulation of *o2* downstream targets, i.e., zein proteins, in the long term may prove more effective than classical methods that have focused on changing upstream controlling factors (1). An opaque seed phenotype is also conditioned by PPDK deficiency in rice (24), although it has clear distinctions from maize. Specifically, mutation of the rice *pdk1* homolog caused the phenotype, whereas maize *pdk1* is a minor contributor to total endosperm PPDK, and the opaque phenotype was observed only when both *pdk1* and *pdk2* function were eliminated.

This genetic analysis confirms proteomics data (22, 32) showing that the great majority of PPDK is specified by *pdk2* in endosperm and *pdk1* in leaf. The *pdk1* and *pdk2* products in endosperm are redundant with respect to maintenance of vitreous endosperm character. This implies that PPDK activity in wild-type endosperm is in excess of that necessary for normal vitreousness and that the minor amount specified by *pdk1* is sufficient for this function. In contrast, residual leaf PPDK specified by *pdk2* cannot compensate for loss of *pdk1*. This likely results from tissue-specific gene expression because the *pdk1* product is present in mesophyll, the site of PPDK function in C4 metabolism, whereas the *pdk2* product accumulates in bundle sheath cells (32). Subcellular localization should also be considered as an explanation for the specific function of *pdk1* because one of the transcript classes from that gene encodes a plastidial protein whereas the *pdk2* mRNA lacks coding sequence for a plastid transit peptide (25, 39). Subcellular localization of the *pdk2* product requires further investigation, however, because in contrast to bioinformatic prediction of cytosolic location, it was specifically detected within chloroplasts (32), in complexes with plastidial proteins (3), and in the interior of starch granules (40).

Increased steady-state concentration of five glycolytic intermediates, including PEP, provides internally consistent evidence that PPDK acts in the glycolytic direction in maize endosperm and that flux through that pathway is reduced in its absence. The large fold-change in DHAP, together with elevated PEP, agrees with previous findings that the latter can competitively inhibit triose phosphate isomerase (41), which is needed for DHAP to continue through glycolysis. The reason pyruvate that is not decreased even though PEP is elevated is unknown, but could involve one of several alternative pathways.

The hypothesis that PPDK is a component of glycolysis necessary for endosperm ATP supply is inconsistent with the results presented here. Total biomass accumulation is normal in PPDK-deficient endosperm, implying that ATP supply through kernel development is not reduced to the extent that it limits anabolic processes. PPDK, therefore, does not replace pyruvate kinase in glycolysis as it does in some microbes, nor does it overlap with pyruvate kinase in glycolytic function to the extent that it is required for a major portion of the ATP supply needed for grain fill.

The hypothesis that PPDK regulates net division between starch and storage protein biosynthesis (3, 21) also is inconsistent with the results. Endosperm starch and total N levels are not altered in transgenic segregants. Normal division in total flux between those two storage pathways, therefore, does not require PPDK and accordingly does not depend on PPi generated by PPDK. The data do not rule out the possibility that PPDK could affect other as yet unidentified aspects of cellular function through a role in PPi homeostasis. This could not be resolved because variable recovery during metabolite extraction prevented reproducible PPi quantification. Regulation by PPDK-generated PPi within amyloplasts must also be considered because subcellular localization of the enzyme is not fully resolved and it likely resides in multiple compartments.

The data are consistent with the hypothesis that PPDK functions to mediate endosperm energy charge by adjusting ATP availability relative to AMP or ADP, and this in turn influences metabolic fluxes. Reduced flux through glycolysis in endosperm lacking PPDK is evident from statistically significant buildup of five intermediates from Glc-1-P to PEP (38). AMP, UMP, and CMP were all detected independently in nontargeted metabolite analyses as significantly elevated compounds, supporting the conclusion that energy charge is altered in the absence of PPDK. This is further supported by significant reduction in ATP content in transgenic endosperm compared with normal. Various central metabolism enzymes are responsive to the availability of specific phosphorylated adenylates, so multiple flux adjustments could respond to PPDK activity. Energy charge in maize endosperm is known to fluctuate both through the diurnal cycle and over development (42), and PPDK could be involved in either effect.

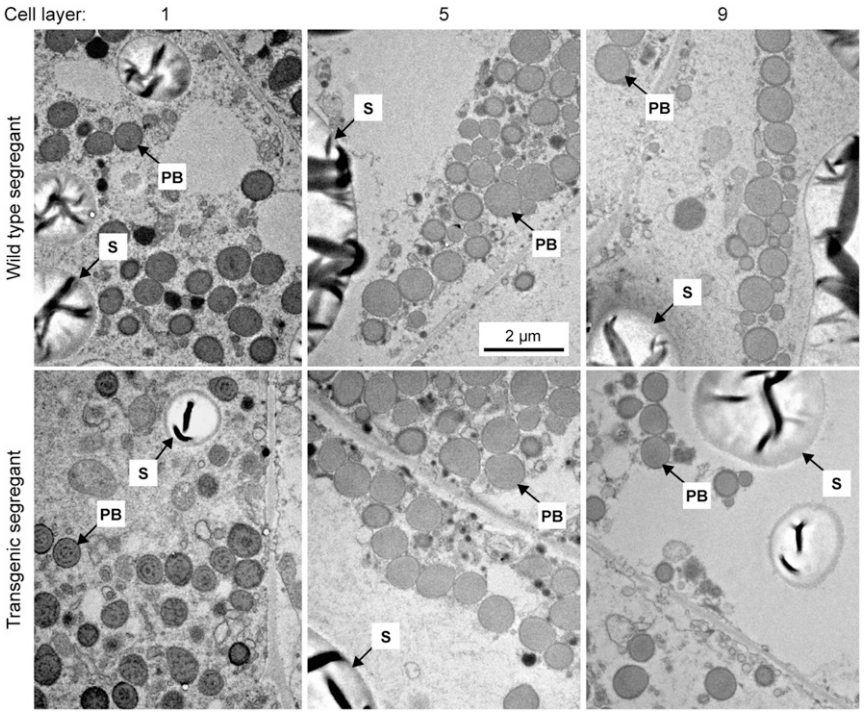

Fig. 5. TEM visualization of 20-DAP endosperm. Sibling endosperms from the same ear segregating for transgene *27PDKRi #33* were fixed, embedded, sectioned, stained with uranyl acetate, and visualized by electron microscopy. Cell layers were determined by overlapping TEM images of sequential sections (*SI Appendix, SI Materials and Methods* and Fig. S7*A*). Layer 1 is subaleurone. (Scale bar for all images, 2 μm.) PB, protein body; S, starch granule.

The need for regulation of glycolytic flux could relate to the hypoxic nature of maize endosperm (20). Proteomics data indicate a shift toward increased glycolytic enzyme abundance relative to citric acid cycle constituents as development proceeds in cereal endosperm (43, 44). Before changes in enzyme populations by gene expression mechanisms, PPDK can mediate short-term adjustments of metabolic fluxes by allosteric regulation responsive to energy charge. Additionally, there may be local variation in pathways that generate ATP necessary for starch-, amino acid-, and protein biosynthesis depending on whether O_2 is available for oxidative metabolism in the mitochondria or, alternatively, if fermentative processes must assume that role.

The reason that deficiency of a metabolic enzyme causes disruption of vitreous endosperm formation remains to be determined. Connection between glycolysis and endosperm character, particularly involving PPi-metabolizing enzymes, was demonstrated previously by finding increased expression of PPi-dependent phosphofructokinase, a glycolytic enzyme thought to result in elevated ATP yield, as a factor in restoring vitreousness to *o2*- mutants in quality protein maize (45). One possible explanation is that zein precursor transport across the endoplasmic reticulum membrane is particularly sensitive to ATP steady-state level. This likely does not explain the opaque phenotype caused by PPDK loss because there is no obvious alteration in protein body morphology or decrease in zein abundance. Another possibility is that vitreousness requires synthesis of starch granules and protein bodies at specific relative rates. The rates of formation of each class of storage structure is determined in part by fluxes through distinct metabolic pathways. Regulation of glycolysis by PPDK, as demonstrated here, may be required to achieve the normal balance of flux between starch and amino acid biosynthesis. Without PPDK the glycolytic rate is altered, and this may disrupt the normal rate of protein body formation and in turn cause the opaque phenotype. This could occur even though the total amount of starch and zein protein synthesized, and presumably protein body abundance, eventually reaches the same ratio as in normal endosperm.

Reduced granule size in altered PPDK conditions, when total starch content does not change, implies more frequent granule initiation. The mechanism explaining this effect remains unknown but may relate to direct interaction between PPDK and SSIII (3), the latter having been implicated in granule initiation in *Arabidopsis* leaf (46). Reduced starch granule size in transgenic endosperm may also be a factor in determining vitreousness. This is unlikely to fully explain the effects of PPDK deficiency, however, because other mutations affect granule size without causing an opaque phenotype (47). Another unknown is the reason that *pdk2*– mutants exhibit increased density predicted by NIR, whereas the RNAi transgenes cause density decreases. The observation suggests that the effects of very low PPDK activity in *pdk2*- mutants may be different from the effects of no PPDK activity, at least with respect to how endosperm storage materials are packed.

In summary, this study shows that maize endosperm PPDK affects glycolytic flux without impacting net biomass deposition. The data rule out two extant hypotheses: specifically, that PPDK is a core glycolytic enzyme and that it determines starch/protein ratios in mature endosperm. A growing body of evidence indicates connection between central metabolic processes and formation of vitreous endosperm, a critical component of beneficial grain quality. Control of endosperm development pertinent to both kernel hardness and nutritional quality by *o2* and related transcription factors could thus include storage protein constituency through effects on zeins, starch through effects on SSIII, and other biosynthetic enzymes and metabolic fluxes through control of PPDK expression.

Materials and Methods

Genetic Nomenclature. Gene loci are designated by small letters in italics, e.g., *pdk1* or *pdk2*. Nonmutant alleles are designated by initial capital letters in the name, e.g., *Pdk1* or *Pdk2*. Specific alleles are designated by the gene locus name followed by a dash and an allele designator, e.g., *pdk1-MuEx10* or *pdk2-DsEx4*, and generalized loss-of-function alleles are indicated by a dash without an allele designator following the gene locus name, e.g., *pdk1-* or *o2-*.

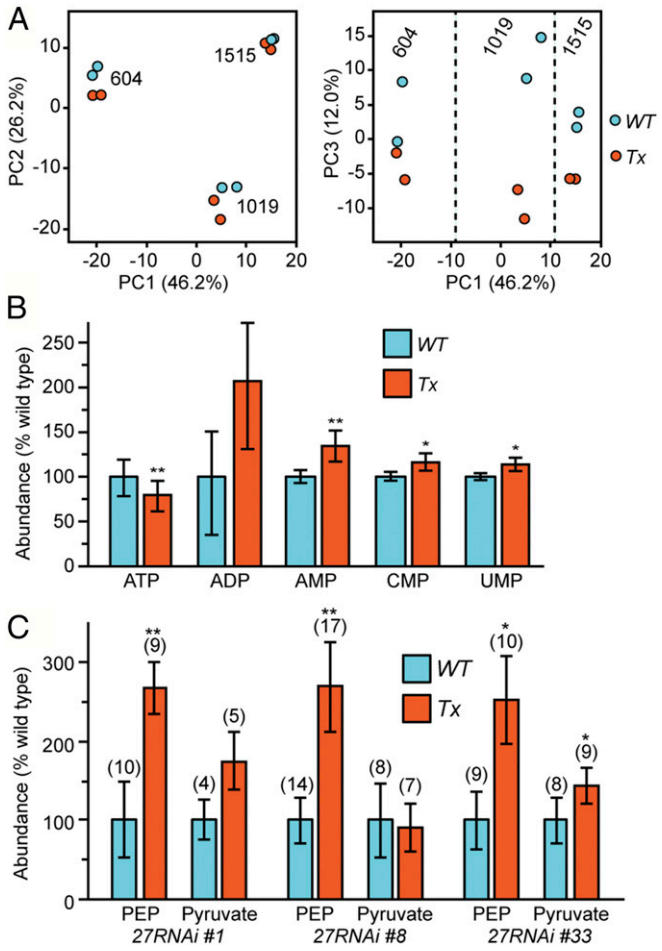

Fig. 6. Relative metabolite levels. (*A*) PCA of samples from three ears showing score plots for negative ions. The parent ear of each pool is indicated. Ear 604 is segregating for transgene *27PDKRi #1* in the B73 (BC3) background, grown in summer 2013. Ear 1019 is segregating for transgene *27PDKRi #1* in the B73 (BC5) background, grown in summer 2014. Ear 1515 is segregating for transgene *27PDKRi #33* in the W64A (BC6) background, grown in summer 2014. (*B*) Adenylate fold-changes. Relative ADP and AMP levels were determined by RPLC-MS, and ATP was quantified enzymatically. Average ATP content in wild-type endosperm was 0.122 ± 0.026 pmol/mg dry weight. Error bars indicate SD, single asterisks indicate statistical significance at $P < 0.03$, and double asterisks indicate significance at $P < 0.007$. ATP values are from 20 biological replicates of each genotype, and other values are from four replicates of each class. (*C*) PEP and pyruvate fold-changes were measured by GC-MS. Numbers in parentheses indicate biological replicates of individual kernels. Asterisks are as in *B*.

Metabolite Measurements. Kernels were retrieved from −80 °C storage, and pericarp and embryo were removed quickly to prevent thawing. Endosperms were immediately frozen in liquid N_2 and then returned to −80 °C for interim storage, while genotypes were determined from embryo DNA.

RPLC-MS nontargeted metabolomics. Endosperms were lyophilized, powdered in a bead beater for 60 s using a 5-mm stainless steel ball, and stored at −80 °C until extraction at room temperature. Tissue from five kernels was pooled, and then 30-mg samples were combined in a microcentrifuge tube with 20 μL of Daily Internal Standard Mix, 750 μL of methanol, and 750 μL of 10 mM $(NH_4)_2SO_4$. Samples were vortexed for 1 min and then sonicated for 10–20 min. Insoluble materials were removed by centrifuging at 17,000 × *g* for 10 min.

Electrospray ionization RPLC-MS used a Dionex UPHLC chromatography system and a Thermo Q Exactive Oribtrap mass spectrometer at the Southeast Center for Integrative Metabolomics. Chromatographic separation utilized an ACE 2.1- × 100-mm Excel 2 C_{18}-PFP column with a 2.0-μm particle size (ACE no. EXL-1,010–1,002 U), preceded by a Halo C18-PFP guard column, and a binary solvent gradient (A, 0.1% formic acid in H_2O; B, 100% acetonitrile) at a flow rate of 350 μL/min. After sample injection (2 μL for positive ion mode, 4 μL for negative ion mode) with 100% solvent A, a 10-min linear gradient to 80% solvent B was commenced at 3 min. After holding at 80% solvent B for 3 min, the column was returned to 100% solvent A by a 0.5-min linear gradient and then re-equilibrated in 100% solvent A. Probe temperature was 350 °C, spray voltage was 3,500 V, and capillary temperature was 320 °C. For positive-ion mode, the sheath, auxiliary, and spare gas were 40, 10, and 1, respectively; for negative-ion mode, they were 45, 10, and 1, respectively. Sample sets were begun with three blank runs, one neat Quality Control (QC) mixture and one Pooled Quality Control (PQC) sample. After 10 unknowns had been analyzed, one blank, one neat QC, and one PQC sample were run before the next set of unknowns.

RPLC-MS data were processed by converting .raw files to .MZxml files using MZmine (48). After further processing with MZmine, higher-level statistical analyses used MetaboAnalyst 3.0 (49). Specific mass features that correlate with genotype were identified based on PCA loading factors, partial least squares-discriminant analysis variable importance in projection (VIP) scores, and significant fold-change in abundance between classes. Features in the top 10% of both PCA loading factor and VIP score, and that differed significantly between classes at Ps < 0.04 ($n = 4$ for each class), were considered

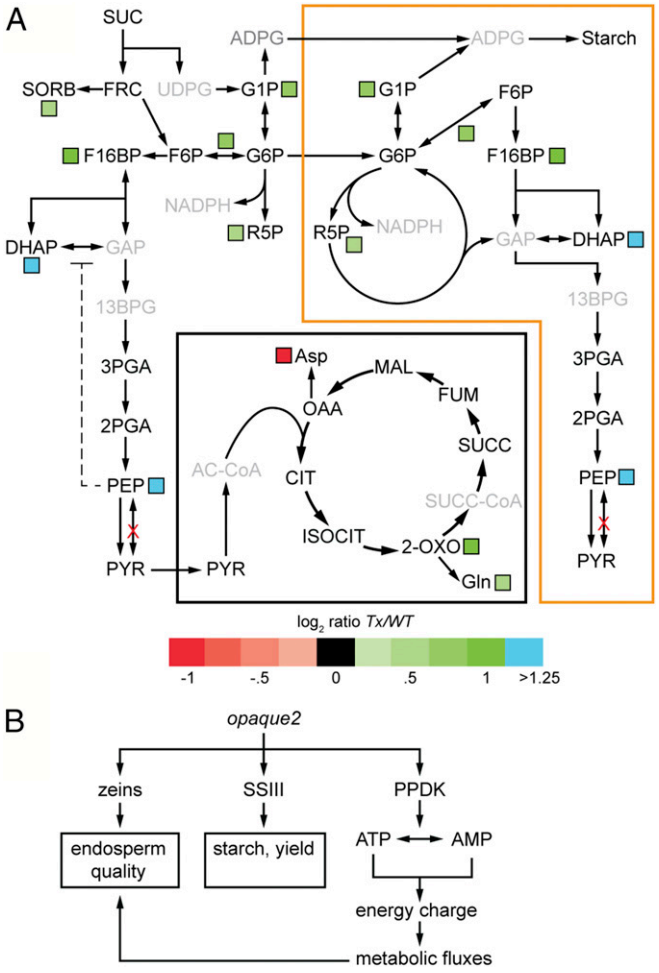

Fig. 7. Metabolome map and model of proposed endosperm PPDK function. (*A*) Metabolome changes in PPDK-deficient endosperm. Combined RPLC-MS, GC-MS, and AELC-MS data are illustrated. Values are $\log_2$ of transgenic endosperm levels relative to normal siblings. Metabolites in gray were not identified, and those in black without an indicated fold-change did not exhibit significant differences. Areas outlined in black and tan represent mitochondria or amyloplasts, respectively, to indicate potential metabolite location, although data are reported for total levels. The dashed line indicates potential inhibition of triose phosphate isomerase by PEP. (*B*) Model for effects of *o2* mediated by PPDK. Three known direct targets of *o2* are indicated. PPDK is proposed to affect vitreous endosperm formation as a downstream effect from a primary role in energy charge adjustment.

to differ based on genotype. Features that did not meet these criteria were considered independent of genotype. Some mass features were identified by comparison with standards characterized in the same LC-MS platform (*SI Appendix*, Table S6).

ATP content. Single lyophilized endosperms were weighed, powdered by shaking with glass beads in a Mini Beadbeater, and then extracted as described (50). Tissue was homogenized in 1.0 mL buffer-saturated phenol (no. BP1750I-400; Fisher), and then 0.5 mL H_2O was added, and the mixture was shaken further and centrifuged for 10 min at 10,000 × *g*. The aqueous phase was extracted in an equal volume of $CHCl_3$. The supernatant was diluted 20-fold in H_2O, and 10-μL samples were assayed in triplicate for ATP content using a bioluminescence detection kit (no. A22066; Molecular Probes). Photon emissions were recorded at 1-s intervals, reading each plate four times, using a Synergy 2 Multi-Mode Microplate Reader. Replicates were averaged, and ATP concentration was determined from a standard curve and normalized to dry weight.

GC-MS–targeted metabolomics. Pyruvate extraction followed the same protocol as for ATP extraction except final extracts were diluted 1:1 with H_2O and ribitol as an internal standard was added to the aqueous phase at 8 μM final concentration. After dilution, 200-μL samples were dried by rotary speed vacuum. Dried samples were suspended in 100 μL of 20 mg/mL methoxyamine in pyridine and incubated at 30 °C for 90 min. Subsequently, 100 μL *N*, *O*-bis(trimethylsilyl) trifluoroacetamide/trimethylchlorosilane (BSTFA/TMCS) (99:1) (Sigma no. 33155-U) was added, and samples were incubated at 80 °C for 60 min.

For PEP and PPi extraction, individual genotyped endosperms were lyophilized, weighed, and homogenized in microcentrifuge tubes with glass beads in a Mini-Beadbeater. Homogenized tissue and glass beads were quantitatively transferred to screw top glass tubes by two 800-μL additions of cold 16% trichloroacetic acid (TCA) in ether (wt/vol) and incubated on ice for 30 min, followed by addition of 1.6 mL of 5 mM NaF, ribitol to 8 μM final concentration, in 16% TCA (wt/vol). Samples were vortexed and incubated on ice for an additional 90 min and then 1.6 mL of H_2O-saturated ether was added. Approximately three-quarters of the top ether layer was removed, and previous steps were repeated totaling four ether washes. Following the ether washes, 500 μL of the aqueous phase was transferred to GC vials and dried by rotary speed vacuum. Dried samples were derivatized by addition of 100 μL BSTFA/TMCS (99:1) and incubation at 80 °C for 60 min.

Electrical ionization GC-MS used the Agilent gas chromatograph model 7890 coupled to the Agilent mass spectrometer model 5975C. Chromatographic separation was on an Agilent 19091J-433 HP-5 3-mx 250 × 0.25-μm column with a helium flow rate of 1 $mL{\cdot}min^{-1}$. Initial oven temperature was 50 °C and was increased 15 $°C{\cdot}min^{-1}$ to 225 °C, followed by an increase of 25 $°C{\cdot}min^{-1}$ to 320 °C, and then maintained at 320 °C. The MS source was 230 °C, and the MS quad was 150 °C, with an electron multiplier voltage of 1,200 V. Injection volumes were 1 μL for pyruvate or 2 μL for PEP or PPi.

PEP, PPi, and pyruvate retention times were evaluated in full-scan mode by addition of pure compounds to endosperm extracts before derivatization. The extracted mass spectrum of each compound was compared with the Golm Metabolome Database mass spectra reference library to verify compound identity by M/Z fragmentation patterns using the National Institute of Standards and Technology Automated Mass spectral Deconvolution and Identification System program. The retention times of PEP, PPi, and ribitol were determined to be ∼12.2, 12.7, and 13.13 min, respectively. Samples evaluated for PEP and PPi content were run in selected-ion monitoring (SIM) mode using M/Z fragments 369, 384, and 225 for PEP and 451, 452, and 466 for PPi. Pyruvate content was evaluated in full-scan mode for all M/Z fragments associated with the compound. Pyruvate was identified at two retention times, ∼7.2 and 12.2 min, determined by derivatization with one or two trimethylsily groups, respectively.

Agilent ChemStation software was used to generate selected ion chromatograms associated with the most abundant ion for each compound at the determined retention times and to integrate the associated peak. Integrations of the two pyruvate peaks were added, and all other integrations were treated individually. Individual sample metabolite responses were normalized to the ribitol internal standard and lyophilized endosperm weight. Normalized response ratios were calculated by dividing the average normalized metabolite response of transgene-containing endosperms by the corresponding sibling wild-type endosperms.

AELC-MS–targeted metabolomics. Methods were as described previously (38). Extraction of lyophilized endosperm was in methanol:chloroform, anion exchange fractionation utilized a Dionex IonSwift MAX-100 column (ThermoFisher Scientific), and MS spectra were recorded with an API 4000 triple quadrupole mass spectrometer (AB Sciex).

Microscopy. Fresh endosperm tissue harvested 20 DAP, or mature tissue imbibed in H_2O for 2 d at 50 °C, was immersed in fixative (2% paraformaldehyde, 3% glutaraldehyde, 0.1 M cacodylate, pH 7.2), dissected by hand with a fresh razor blade under fixative into small pieces, and then fixed and embedded in Spurr's Resin according to standard procedures. Sections of mature tissue including the aleurone layer were prepared for LM. Ordered serial sections of 20-DAP tissue extending from the aleurone toward the center of the starch endosperm were collected for transmission electron microscopy (TEM). LM sections were stained in Epoxy Tissue Stain (#14950; Electron Microscopy Sciences) containing Toluidine blue and basic fuschsin, and TEM sections were stained with uranyl acetate, according to standard procedures.

MRI. MRI data were acquired on a 11.7 tesla AMX instrument (Bruker) with a custom-built birdcage coil and an adjusted NMR 3D radial sequence (repetition time 50 ms, 62,778 spokes, 128 readout points, 16 averages, resolution 120 μm). Total proton spin density (51) was measured within individual intact maize kernels and represented in relative units. Data processing was performed in MATLAB (The Mathworks).

Additional Materials and Methods. *SI Appendix, SI Materials and Methods*, describes the methods used for plant genomic DNA extraction and PCR genotyping, isolation of transposon insertion mutations, generation and characterization of RNAi transgenic plants, immunoblot analyses for PPDK or O2 protein content, enzymatic activity assays, starch quantification, amylopectin chain length distribution, amylose content, granule size distribution, total nitrogen content, zein and nonzein protein content determination by SDS/PAGE or HPLC, and NIR spectroscopy.

ACKNOWLEDGMENTS. We acknowledge the assistance of the Microscopy Facility, Plant Transformation Facility, DNA Facility, and Soil and Plant Analysis Laboratory of Iowa State University and the Southeast Center for Integrated Metabolomics of the University of Florida. Erik Vollbrecht provided assistance with genetic methods for *Ds* insertion mutagenesis of *pdk2*, Chris Chastain provided anti-PPDK antiserum, Yongrui Wu provided anti-O2 antiserum, Tracy Stewart provided expertise for LM and TEM analyses, Ann Perera and Lucas Showman provided expertise for GC-MS analyses, and Eberhard Munz and Peter Jakob provided expertise for the MRI study. The MRI study was supported by the German Plant Phenotyping Network. This research was supported by National Sciences Foundation Grant 17256 and US Department of Agriculture Grant 2011-67003-30215.

1. Zhang Z, Zheng X, Yang J, Messing J, Wu Y (2016) Maize endosperm-specific transcription factors O2 and PBF network the regulation of protein and starch synthesis. *Proc Natl Acad Sci USA* 113:10842–10847.
2. Li C, et al. (2015) Genome-wide characterization of cis-acting DNA targets reveals the transcriptional regulatory framework of opaque2 in maize. *Plant Cell* 27:532–545.
3. Hennen-Bierwagen TA, et al. (2009) Proteins from multiple metabolic pathways associate with starch biosynthetic enzymes in high molecular weight complexes: A model for regulation of carbon allocation in maize amyloplasts. *Plant Physiol* 149: 1541–1559.
4. Holding DR (2014) Recent advances in the study of prolamin storage protein organization and function. *Front Plant Sci* 5:276.
5. Lin Q, et al. (2012) Functional interactions between starch synthase III and isoamylase-type starch-debranching enzyme in maize endosperm. *Plant Physiol* 158:679–692.
6. Wu Y, Holding DR, Messing J (2010) γ-Zeins are essential for endosperm modification in quality protein maize. *Proc Natl Acad Sci USA* 107:12810–12815.
7. Hatch MD, Slack CR (1968) A new enzyme for the interconversion of pyruvate and phosphopyruvate and its role in the C4 dicarboxylic acid pathway of photosynthesis. *Biochem J* 106:141–146.
8. Reeves RE (1968) A new enzyme with the glycolytic function of pyruvate kinase. *J Biol Chem* 243:3202–3204.
9. Wood HG, O'Brien WE, Micheales G (1977) Properties of carboxytransphosphorylase; pyruvate, phosphate dikinase: pyrophosphate-phosphofructikinase and pyrophosphate-acetate kinase and their roles in the metabolism of inorganic pyrophosphate. *Adv Enzymol Relat Areas Mol Biol* 45:85–155.
10. Hatch MD (1987) C4 photosynthesis: A unique blend of modified biochemistry, anatomy and ultrastructure. *Biochim Biophys Acta* 895:81–106.
11. Jenkins CL, Hatch MD (1985) Properties and reaction mechanism of C4 leaf pyruvate, Pi dikinase. *Arch Biochem Biophys* 239:53–62.
12. Kanai R, Edwards GE (1999) The biochemistry of C4 photosynthesis. *C4 Plant Biology*, eds Sage RF, Monson RK (Academic, San Diego), pp 49–87.

13. Taylor L, et al. (2010) Cytosolic pyruvate, orthophosphate dikinase functions in nitrogen remobilization during leaf senescence and limits individual seed growth and nitrogen content. *Plant J* 62:641–652.
14. Eastmond PJ, et al. (2015) *Arabidopsis* uses two gluconeogenic gateways for organic acids to fuel seedling establishment. *Nat Commun* 6:6659.
15. Janacek SH, et al. (2009) Photosynthesis in cells around veins of the C(3) plant *Arabidopsis thaliana* is important for both the shikimate pathway and leaf senescence as well as contributing to plant fitness. *Plant J* 59:329–343.
16. Chastain CJ, et al. (2011) Functional evolution of C(4) pyruvate, orthophosphate dikinase. *J Exp Bot* 62:3083–3091.
17. Mertens E (1993) ATP versus pyrophosphate: Glycolysis revisited in parasitic protists. *Parasitol Today* 9:122–126.
18. Lasanthi-Kudahettige R, et al. (2007) Transcript profiling of the anoxic rice coleoptile. *Plant Physiol* 144:218–231.
19. Huang S, Colmer TD, Millar AH (2008) Does anoxia tolerance involve altering the energy currency towards PPi? *Trends Plant Sci* 13:221–227.
20. Rolletschek H, Koch K, Wobus U, Borisjuk L (2005) Positional cues for the starch/lipid balance in maize kernels and resource partitioning to the embryo. *Plant J* 42:69–83.
21. Méchin V, Thévenot C, Le Guilloux M, Prioul JL, Damerval C (2007) Developmental analysis of maize endosperm proteome suggests a pivotal role for pyruvate orthophosphate dikinase. *Plant Physiol* 143:1203–1219.
22. Walley JW, et al. (2013) Reconstruction of protein networks from an atlas of maize seed proteotypes. *Proc Natl Acad Sci USA* 110:E4808–E4817.
23. Chastain CJ, Heck JW, Colquhoun TA, Voge DG, Gu XY (2006) Posttranslational regulation of pyruvate, orthophosphate dikinase in developing rice (*Oryza sativa*) seeds. *Planta* 224:924–934.
24. Kang HG, Park S, Matsuoka M, An G (2005) White-core endosperm *floury endosperm-4* in rice is generated by knockout mutations in the C-type pyruvate orthophosphate dikinase gene (OsPPDKB). *Plant J* 42:901–911.
25. Sheen J (1991) Molecular mechanisms underlying the differential expression of maize pyruvate, orthophosphate dikinase genes. *Plant Cell* 3:225–245.
26. Ahern KR, et al. (2009) Regional mutagenesis using *Dissociation* in maize. *Methods* 49:248–254.
27. Gustin JL, et al. (2013) Analysis of maize (*Zea mays*) kernel density and volume using microcomputed tomography and single-kernel near-infrared spectroscopy. *J Agric Food Chem* 61:10872–10880.
28. Spielbauer G, et al. (2009) High-throughput near-infrared reflectance spectroscopy for predicting quantitative and qualitative composition phenotypes of individual maize kernels. *Cereal Chem* 86:556–564.
29. Majeran W, et al. (2010) Structural and metabolic transitions of C4 leaf development and differentiation defined by microscopy and quantitative proteomics in maize. *Plant Cell* 22:3509–3542.
30. Li G, et al. (2014) Temporal patterns of gene expression in developing maize endosperm identified through transcriptome sequencing. *Proc Natl Acad Sci USA* 111: 7582–7587.
31. Chen J, et al. (2014) Dynamic transcriptome landscape of maize embryo and endosperm development. *Plant Physiol* 166:252–264.
32. Friso G, Majeran W, Huang M, Sun Q, van Wijk KJ (2010) Reconstruction of metabolic pathways, protein expression, and homeostasis machineries across maize bundle sheath and mesophyll chloroplasts: Large-scale quantitative proteomics using the first maize genome assembly. *Plant Physiol* 152:1219–1250.
33. Woo Y-M, Hu DW-N, Larkins BA, Jung R (2001) Genomics analysis of genes expressed in maize endosperm identifies novel seed proteins and clarifies patterns of zein gene expression. *Plant Cell* 13:2297–2317.
34. Coleman CE, Lopes MA, Gillikin JW, Boston RS, Larkins BA (1995) A defective signal peptide in the maize high-lysine mutant *floury 2*. *Proc Natl Acad Sci USA* 92: 6828–6831.
35. Stelpflug SC, et al. (2016) An expanded maize gene expression atlas based on RNA-sequencing and its use to explore root development. *Plant Genome* 9.
36. Bergin CJ, Pauly JM, Macovski A (1991) Lung parenchyma: Projection reconstruction MR imaging. *Radiology* 179:777–781.
37. Hackstadt AJ, Hess AM (2009) Filtering for increased power for microarray data analysis. *BMC Bioinformatics* 10:11.
38. Schwender J, et al. (2015) Quantitative multilevel analysis of central metabolism in developing oilseeds of oilseed rape during in vitro culture. *Plant Physiol* 168:828–848.
39. Parsley K, Hibberd JM (2006) The *Arabidopsis* PPDK gene is transcribed from two promoters to produce differentially expressed transcripts responsible for cytosolic and plastidic proteins. *Plant Mol Biol* 62:339–349.
40. Borén M, Larsson H, Falk A, Jansson C (2004) The barley starch granule proteome: Internalized granule polypeptides of the mature endosperm. *Plant Sci* 166:617–626.
41. Grüning NM, Du D, Keller MA, Luisi BF, Ralser M (2014) Inhibition of triosephosphate isomerase by phosphoenolpyruvate in the feedback-regulation of glycolysis. *Open Biol* 4:130232.
42. Scott MP (2000) Diurnal and developmental changes in levels of nucleotide compounds in developing maize endosperms. *Plant Cell Environ* 23:1281–1286.
43. Prioul JL, et al. (2008) A joint transcriptomic, proteomic and metabolic analysis of maize endosperm development and starch filling. *Plant Biotechnol J* 6:855–869.
44. Xu SB, et al. (2008) Dynamic proteomic analysis reveals a switch between central carbon metabolism and alcoholic fermentation in rice filling grains. *Plant Physiol* 148: 908–925.
45. Guo X, et al. (2012) Pyrophosphate-dependent fructose-6-phosphate 1-phosphotransferase induction and attenuation of Hsp gene expression during endosperm modification in quality protein maize. *Plant Physiol* 158:917–929.
46. Szydlowski N, et al. (2009) Starch granule initiation in Arabidopsis requires the presence of either class IV or class III starch synthases. *Plant Cell* 21:2443–2457.
47. Kubo A, et al. (2010) Functions of heteromeric and homomeric isoamylase-type starch-debranching enzymes in developing maize endosperm. *Plant Physiol* 153: 956–969.
48. Pluskal T, Castillo S, Villar-Briones A, Oresic M (2010) MZmine 2: Modular framework for processing, visualizing, and analyzing mass spectrometry-based molecular profile data. *BMC Bioinformatics* 11:395.
49. Xia J, Sinelnikov IV, Han B, Wishart DS (2015) MetaboAnalyst 3.0: Making metabolomics more meaningful. *Nucleic Acids Res* 43:W251–W257.
50. Chida J, Yamane K, Takei T, Kido H (2012) An efficient extraction method for quantitation of adenosine triphosphate in mammalian tissues and cells. *Anal Chim Acta* 727:8–12.
51. Levitt M (2008) *Spin Dynamics: Basics of Nuclear Magnetic Resonance* (John Wiley & Sons Ltd., West Sussex, UK), 2nd Ed.